



CYCLIC RESPONSE OF A LOW INVASIVITY BRACING SYSTEM FOR THE PASSIVE CONTROL OF FRAMED STRUCTURES

Juan Enrique MARTINEZ-RUEDA¹

SUMMARY

This article reports an experimental program conducted to assess the adequacy of low invasivity dissipative bracing under reversed cyclic loading of high amplitude. Test results are presented for a reduced scale tension-compression bracing system that incorporates either friction or yield devices. The results obtained highlight the ability of the proposed bracing system to provide a framed structure with reliable supplemental sources of both, hysteretic damping and non-decaying lateral strength.

INTRODUCTION

A number of hysteretic devices of yield and friction type have been developed over the last two decades [1]. Generally these devices are incorporated as integral parts of bracing systems to create a *dissipative bracing*. Devices used in this way perform as enhanced semirigid connections or joint elements with high energy-dissipation capacity, and are designed to deform during severe seismic actions before yielding or buckling takes place in the primary members of the structure.

When the addition of dissipative bracing is considered as a technique to enhance seismic performance a number of problems may arise. These are related to the structural invasion of the bracing characterized by critical alterations to the original building layout and severe disturbance to building occupants. An alternative solution to reduce the impact of building alterations is to use a dissipative bracing with a geometry of low invasivity [2,3]. Figure 1 exemplifies this type of dissipative bracing. It is observed that the adopted geometry favors the activation of hysteretic devices which work as end connections for the bracing members. The inclination angle of the bracing members must be decided in accordance with the client requirements for aesthetics and space. In this way, the designer has some control over the loss of space due to the installation of dissipative bracing. In contrast, cross bracing or Chevron bracing geometries are less flexible to allow for an easy installation of doors or to provide circulation through the open space originally available in the structure.

¹ Civil Engineering Division, School of the Environment, University of Brighton

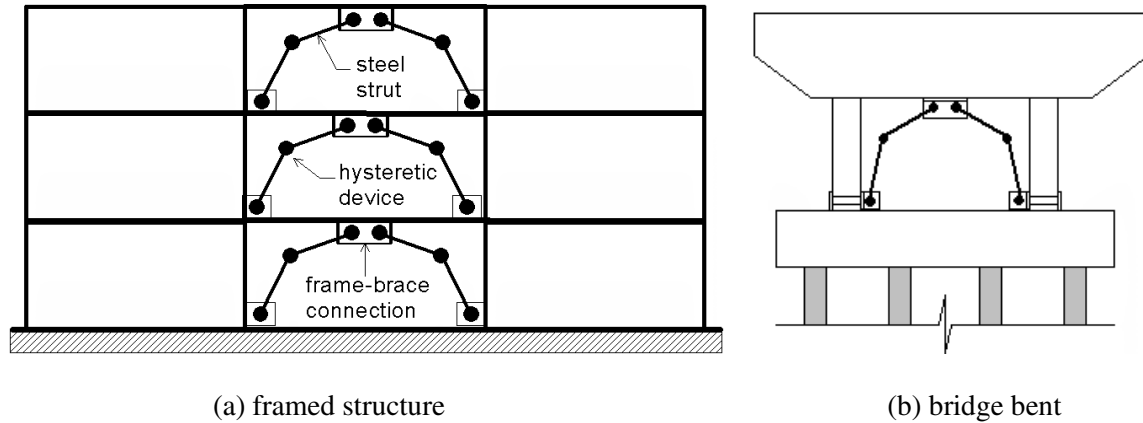


Figure 1. Dissipative bracing of low invasivity installed in different type of structures.

Objectives and scope

This article describes the results of an experimental program on the cyclic behavior of a dissipative bracing system. The bracing incorporates either yield or frictional devices and adopts a geometry of low invasivity. Several tests were conducted to assess the feasibility of designing and constructing effective hysteretic devices of low cost without resorting to non-essential high technology.

DISSIPATIVE BRACING WITH FRICTION DEVICES

The incorporation of rotational friction devices into dissipating bracing of low invasivity has been the object of previous analytical studies [2,3]. Figure 2 shows a framed building in its original and redesigned condition studied by the author under the action of natural earthquake records. The structure, in its original condition, is a gravity-loaded-designed RC frame studied by Hoffman et al. [4].

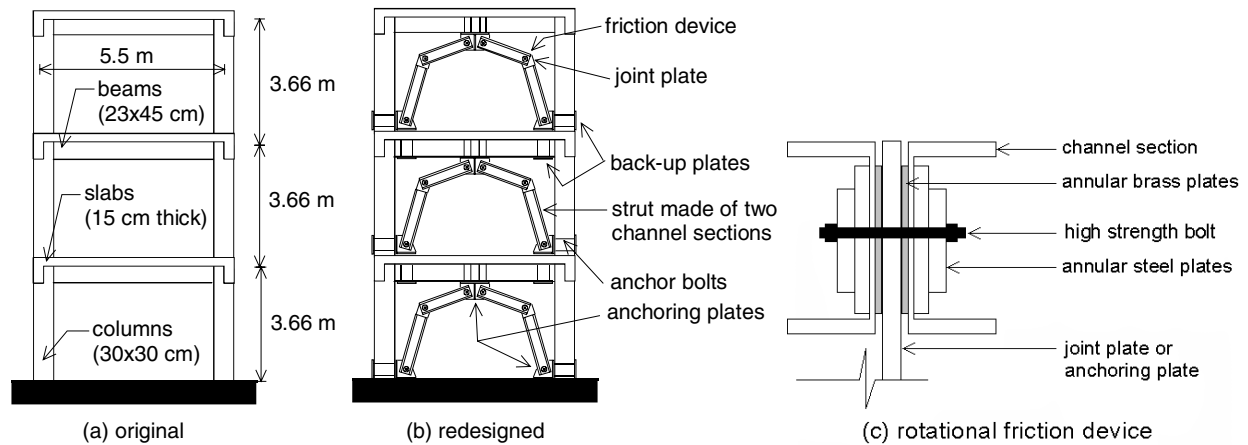


Figure 2. Gravity-loaded-designed RC frame with and without frictional dissipative

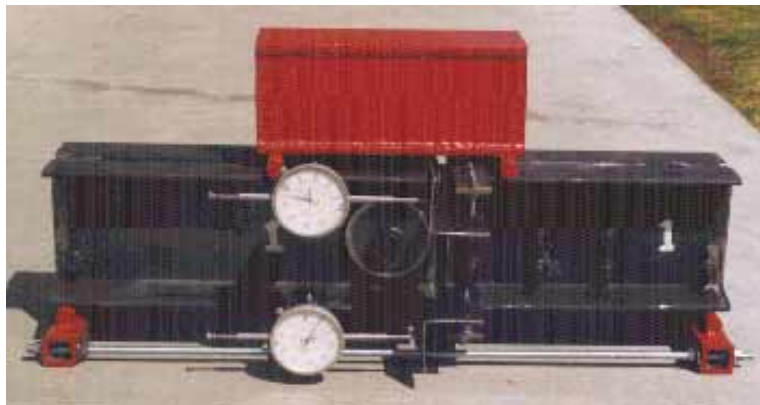
The friction devices shown in Figure 2c consist of annular brass plates and steel plates joint by high strength bolts. The rotational strength of the device is provided by the friction developed between the brass and the steel surfaces in contact. For analysis, the rotational response of the devices was assumed elastic-perfectly plastic with very high initial stiffness. A series of nonlinear time-history seismic analyses of the structure with and without dissipative bracing confirmed the efficiency of the proposed dissipative

bracing [2,3]. In particular, it was found that the dissipative bracing of low invasivity promotes consistent significant reductions of ductility demands with low increase of base shear.

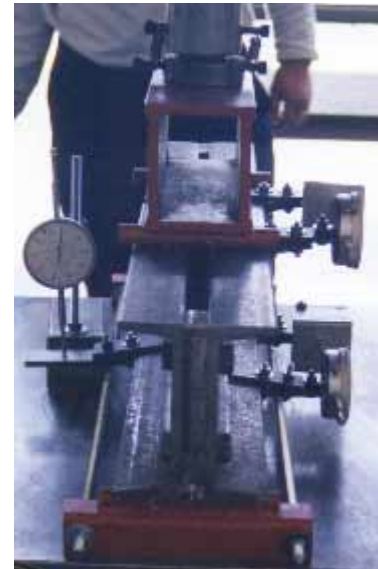
The design and modeling of the above dissipative bracing and its devices was based on first principles and on assumptions consistent with the experimental behavior of friction devices reported by several authors. Nevertheless, experimental assessment was identified as further research needed to address practical issues related to the design and implementation of the proposed dissipative bracing and its devices. Furthermore, the consideration of yield devices was visualized as a viable idea to explore.

Experimental assessment of rotational friction devices under monotonic loading

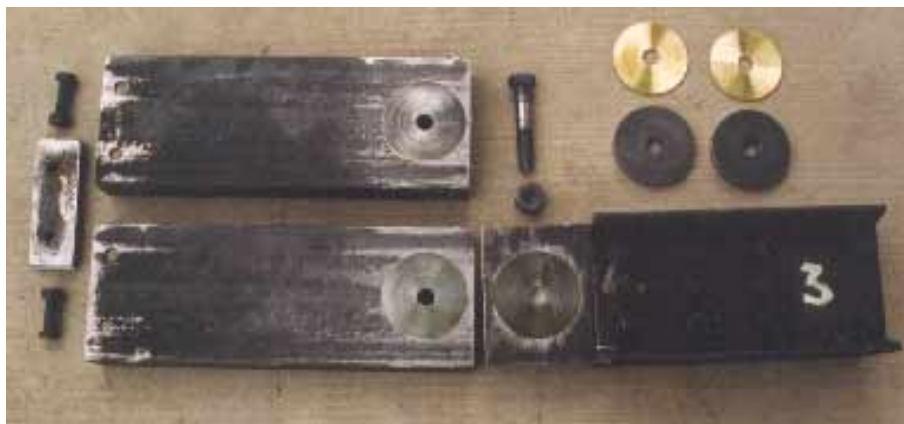
To define a practical tuning procedure for the rotational friction devices these were tested under monotonic and cyclic loading. Figure 3 shows a test specimen consisting of a steel beam with a friction device at midspan. The yield flexural strength of the beam (made of channel sections) corresponds roughly to four times the maximum strength (resisted moment by friction) expected in the friction device. The brass annular plates were 1/8" (3.2 mm) thick with internal and external diameters equal to 2 cm and 9 cm, respectively.



(a) Lateral view of tested beam showing dial gages to measure device rotations



(b) Transverse view of tested beam under vertical load



(c) Assembly components of the above beam

Figure 3. Simply supported steel beam with rotational friction device at midspan.

Four beam specimens were tested to assess the influence of the quality of the contact surfaces on the frictional strength of the devices. All specimens had the same dimensions but different surface qualities of their frictional materials (i.e. the channel webs, the connection plates and the brass plates in contact). The following three cases for the quality of the surfaces in contact were considered:

1. raw surfaces, i.e. with no treatment applied to the surface
2. surfaces manually polished using fine grain sand paper
3. surfaces manually polished using coarse grain sand paper

Before connecting the devices and the steel profiles, the contacting surfaces were cleaned using a solvent (thinner) to avoid any possible lubricating effect from oil stains left during the fabrication (perforation of bolt holes) of the specimens.

Third point loading was applied to all specimens as indicated in Figures 1a-b. To control the tension force in the device bolt a torque spanner was used to tie the nut bolt. This type of spanner has a torque-limiting mechanism which can be set to a predetermined value. The maximum capacity of the torque spanner available for the test was about 800 N-m. A total of 32 monotonic tests were conducted on the beam specimens; further details of these tests are given elsewhere [5].

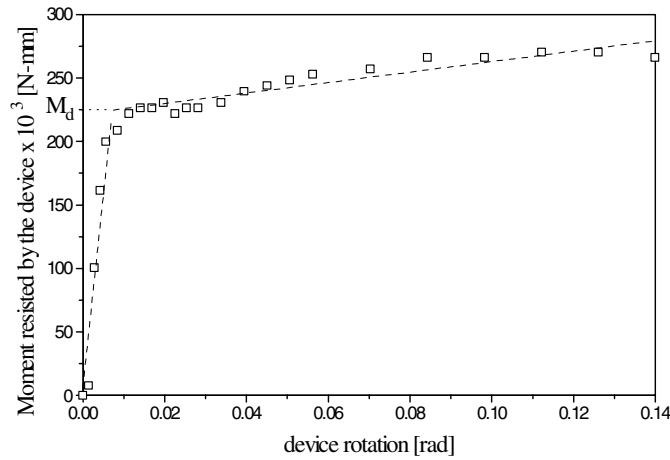


Figure 4. Monotonic response of rotational friction device

Figure 4 shows a typical monotonic response observed during the tests. This figure reveals that the friction device responds in close agreement with a bilinear model. The moment M_d represents the effective yield strength of the device; in other words M_d can be considered as the moment resisted by the device at the moment when friction sliding between brass and steel begins.

It was found that the best model to predict the capacity of the rotational devices was that for friction disks under uniform pressure. The capacity m_d (moment strength) of this type of disk is given by:

$$m_d = \frac{F_t \mu}{3} \frac{\phi_e^3 - \phi_i^3}{\phi_e^2 - \phi_i^2} \quad (1)$$

where F_t is the normal force acting on the disk; μ is the friction coefficient between the materials in contact; ϕ_e and ϕ_i are internal and external diameters of the disk (here a brass annular plate), respectively.

Eq. (1) is valid for two surfaces in contact; for the devices used in this study that incorporate 2 brass annular plates there will be 4 surfaces in contact. Therefore, the capacity M_d of the device (moment strength) will be:

$$M_d = 4m_d \quad (2)$$

To extrapolate the results from the above monotonic tests it is necessary to use the same frictional materials, the same bolt and the same torque spanner to obtain reliable results. Hence, assuming a capacity m_d has been empirically calibrated for a disk with dimensions ϕ_e and ϕ_i , the capacity of a disk with dimensions ϕ'_e and ϕ'_i can be estimated as:

$$m'_d = \frac{F_i \mu \phi_e^3 - \phi_i^3}{3 \phi_e^2 - \phi_i^2} \frac{\left(\frac{\phi_e'^3 - \phi_i'^3}{\phi_e'^2 - \phi_i'^2} \right)}{\left(\frac{\phi_e^3 - \phi_i^3}{\phi_e^2 - \phi_i^2} \right)} \quad (3)$$

Accounting for Eq. (1) into Eq. (3) :

$$m'_d = m_d \frac{(\phi_e'^3 - \phi_i'^3)(\phi_e^2 - \phi_i^2)}{(\phi_e^3 - \phi_i^3)(\phi_e'^2 - \phi_i'^2)} \quad (4)$$

Therefore, Eq. (4) can be used as a design tool to define the device strength based on the test results of beams under third point loading with a rotational friction device at midspan.

Cyclic testing of the rotational friction devices

The above specimens used for monotonic tests were adapted to be used for cyclic tests as illustrated in Figure 5. The history of deformations imposed on the devices for the cyclic tests consisted of twenty cycles of 0.09 radians. The amplitude of this deformation was defined primarily by the dimensions of the loading system. Nevertheless, this rotation is far greater than that expected in the devices when these are installed into a structure that experiences a drift in excess of 4%. On the other hand, the large number of cycles of very high amplitude of the load history is expected to produce both peak and cumulative ductility demands greater than those imposed by a severe earthquake.

Several combinations for the frictional surfaces were also considered. Figure 6a exemplifies the observed cyclic response of a rotational friction device. In general, the hysteretic loops show irregularities but their overall shape is rectangular. However, loads during the test were not measured with a load cell. Instead, loads were estimated from direct readings of the jack pressure. On the other hand, the jack was manually operated and hence neither the displacements nor the velocity of loading could be controlled with much precision. Despite the limitations of the loading system and the irregularities of the hysteretic loops, the rate of energy dissipation was not severely affected as observed in Figure 6b. In fact, this virtually constant rate of energy dissipation observed in the cyclic tests confirms the validity of previous analytical studies in which the response of the rotational friction devices has been assumed elastic-perfectly plastic [2,3,6,7].



Figure 5. Cyclic testing of an individual rotational friction device

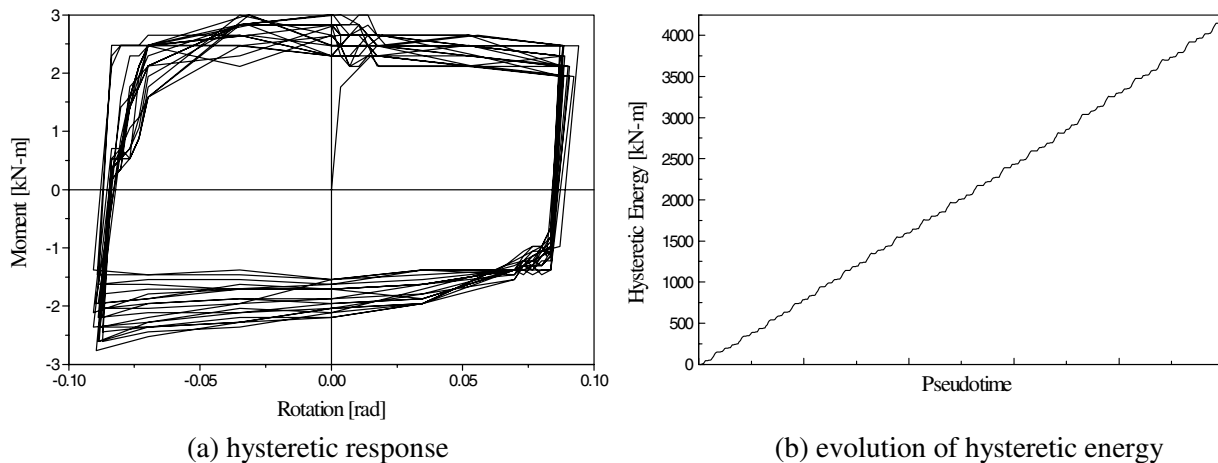


Figure 6. Cyclic performance of an individual friction device

After each test, devices were disassembled and contact surfaces visually examined. Both steel and brass contact surfaces showed no sign of wear due to friction. The high strength bolt did not present signs of overstress due to shear or direct bearing. Also, the bolt hole was not distorted due to yielding in its vicinity. These observations confirmed that the rotational strength of the device was effectively controlled by the friction developed between the brass and the steel surfaces.

Cyclic testing of a dissipative bracing of low invasivity with rotational friction devices

Figure 7 shows a dissipative bracing system of low invasivity with rotational friction devices, tested under reversed cyclic loading. It can be shown (e.g. using the virtual work method for plastic analysis) that the lateral capacity H of the bracing shown in Figure 7b is defined by the following expression:

$$H = \frac{2M_d e}{L^2} \frac{x}{\sqrt{x^2 + y^2}} \quad (5)$$

where e , x , y and L are dimensions of the half polygonal arch as indicated in Figure 7b.

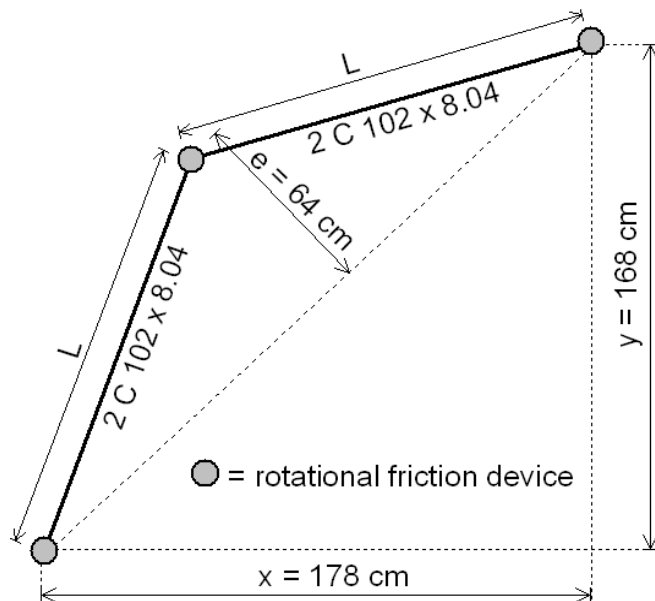
Accordingly, for the design of a complete polygonal bracing arch as those shown in Figures 1 and 2 the lateral strength of the dissipative bracing is given as:

$$H = \frac{4M_d e}{L^2} \frac{x}{\sqrt{x^2 + y^2}} \quad (6)$$

The complementary initial storey stiffness provided by the above dissipative bracing can be estimated assuming the bracing members are rigidly connected before the devices achieve their capacity M_d .



(a) frictional bracing installed into a steel frame with pinned connections



(b) overall dimensions of the frictional bracing

Figure 7. Experimental model of a dissipative bracing of low invasivity with rotational friction devices.



Figure 8. Transverse view of the rotational friction device installed in the dissipative bracing



(a) pinned strut connected to south column



(b) hydraulic jack of double action

Figure 9. Assembly of the manually operated hydraulic system for cyclic loading



(a) lower device



(b) central device



(c) upper device



(d) north column

Figure 10. Instrumentation to measure rotations and displacements in the dissipative bracing

Figure 8 shows a transverse view of the friction devices installed in the dissipative bracing. In terms of its geometry and dimensions, the bracing under testing approaches a 1:2 scale model of one half of the complete polygonal arch used for bracing each storey of the frame shown in Figure 2b. The bracing members were made of two channel steel profiles of 102 mm of depth and unit mass of 8.04 kg/m (2C102x8.04). The internal and external diameters of the brass annular plates were 2 cm and 6 cm,

respectively. The brass plates were left untreated whereas the steel surfaces were polished (close to a mirror-like appearance) with sand paper. The device strength was controlled by the prestressing of a high strength bolt with a diameter of $\frac{3}{4}$ " (19 mm). Each device nut was tied to a torque of 712 N-m. This was the maximum torque that could be applied with the available torque spanner.

The dissipative bracing was installed into a steel frame with pinned connections as indicated in Figure 7a. In this way, the lateral strength and stiffness of the braced frame was controlled by the dissipative bracing alone. The frame was laterally loaded in its south column as indicated in Figure 9. The jack pressures under pulling and pushing actions were measured with two digital manometers with a precision of ± 10 psi (0.069 Mpa).

To measure rotations at each device, mechanical dial gages with a precision of ± 0.01 mm were installed in the dissipative bracing as shown in Figures 10a-c. Lateral frame displacements were measured by a fixed metallic ruler attached to the north frame column as illustrated in Figure 10-d. The ruler had a precision of ± 1.0 mm.

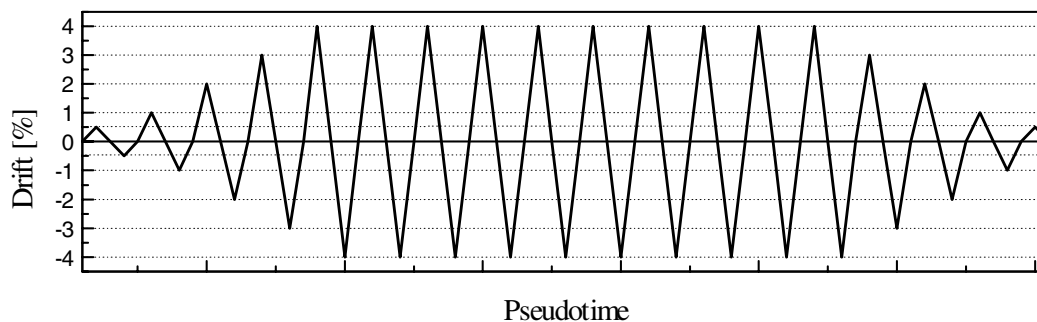


Figure 11. Strength envelope in terms of the lateral force H vs. lateral displacement Δ for the inelastic dual system representing a framed structure with dissipative bracing.

The history of storey displacements applied to the frame is represented in Figure 11. The reversed cyclic loading of this history includes 10 full cycles of displacements with peak amplitude equivalent to a storey drift of 4%. Clearly, the history of lateral displacements imposed on the dissipative bracing exceeds the seismic demands expected on practical earthquake resistant structures.

Results

Figure 12 shows the history of lateral strength of the frictional dissipative bracing under the applied history of displacements. This history reveals a stable response with a slight gain of strength as the number of cycles increases. The strength gain can be associated to the heat generated in the devices as a result of the friction developed between brass and steel. This heat produces expansion primarily in the brass annular plates, and such expansion leads to an increment in the bolt tension that controls the device strength. At the end of the test, devices were disassembled and the frictional surfaces were inspected. No brass or steel powder was found as evidence of excessive wear. It is anticipated that even if some wear could take place during seismic loading, its effect could be effectively counteracted by the expansion due to heat associated with energy dissipation as reported above.

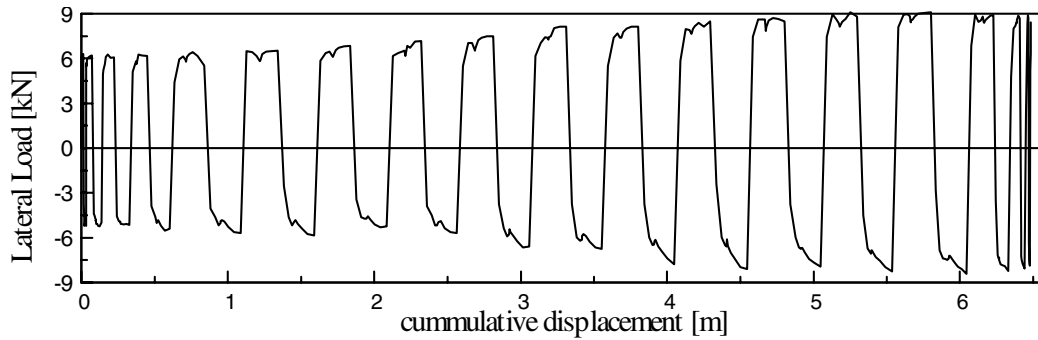


Figure 12. Evolution of lateral strength

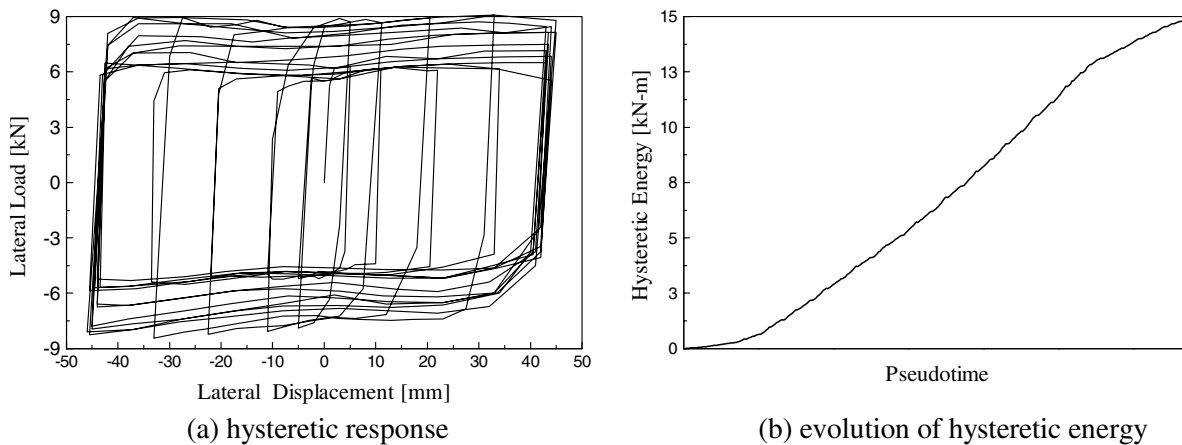


Figure 13. Cyclic performance of the dissipative bracing with rotational friction devices

The hysteretic response of the frictional dissipative bracing is indicated in Figure 13a. The hysteretic loops present a number of irregularities that prevent them from being rectangular as commonly assumed in the modeling of dissipative bracing. Nevertheless, as Figure 13b reveals, the rate of energy dissipation is quite regular. In fact, the slope of the curve of cumulative hysteretic energy is virtually constant, particularly in the region corresponding with the cycles of maximum amplitude of the history shown in Figure 11. This observation validates, once more, the assumption followed in previous analytical studies on the application of rotational friction devices [2,3,6,7].

DISSIPATIVE BRACING WITH YIELD DEVICES

Test specimen and experimental assessment

To assess a yielding alternative of dissipative bracing of low invasivity, the frictional bracing described in previous sections was adapted to accommodate yield devices. Figure 14 shows the yield dissipative bracing together with a sketch of its components and dimensions. The hinges in Figure 14b correspond to the devices of the frictional bracing but now with the bolts sufficiently loose to allow free rotation with negligible friction.

Figure 15 shows the adopted geometry for the yield device. This is a small yielding frame with an elongated “C” shape, and with circular holes at its ends to allow for pinned connections. This device works under a combination flexure and axial compression or axial tension depending on the deflected

shape of the bracing. C-plates have been used in the past as yield devices for dissipative bracing of conventional geometry (chevron bracing) [8].

The design the C-plates shown in Figure 15 is relatively simple (at least under the assumption of small deformations). It can be shown that an equivalent spring joining the pinned connections of the C-plate can be characterized by the following values of strength at first yield P_y and yield stiffness k_y :

$$P_y = \frac{f_y t}{\frac{1}{h_b} + \frac{6L_y}{h_b^2}} \quad (7)$$

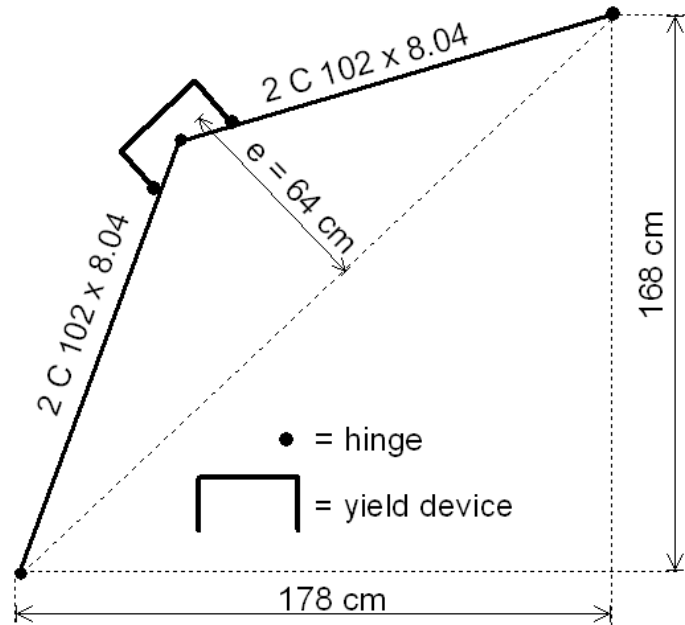
$$k_y = \frac{E t}{\frac{L_x}{h_b} + \frac{12L_x L_y^2}{h_b^3} + \frac{8L_y^3}{h_c^3}} \quad (8)$$

where E is the modulus of elasticity of steel; f_y is the yield strength of the plate; t is the thickness of the plate; and L_x , L_y , h_b and h_c are the dimensions of the C-plate illustrated in Figure 15.

To avoid instability problems, it is recommended to cut the device from a plate of generous thickness. The use of a generous thickness also results in the device having a compact section that favors a good spread of plasticity over a large volume of the device. For the bracing specimen of Figure 14, the C-plates were designed to achieve full plasticity when the peak bending moment in the bracing members is 25% of their yield bending strength. This to guarantee that all the repairable damage and energy dissipation is directed towards the yield devices only.



(a) test specimen



(b) overall dimensions and components

Figure 14. Yield dissipative bracing of low invasivity

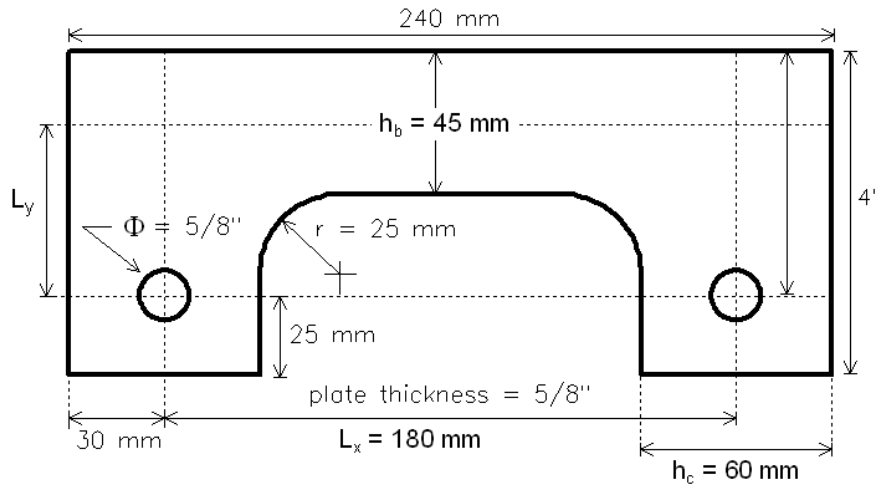


Figure 15. Geometry of the C-plates used as yield devices

To reduce cutting demands, the C-plates were made from commercially available steel strip 4" (101 mm) wide, 5/8" (15.9 mm) thick. Due to the lack of a sophisticated numerically controlled cutting machine, the C-plates were fabricated following the procedure illustrated in Figure 16. Standard tensile tests of the above strip revealed a ductile behavior with an average yield strength of about 300 MPa.

Figure 17 shows the sleeve plates where the C-plates are pin-connected using conventional high strength bolts. In turn, the sleeve plates are welded to the upper and lower flanges of the bracing members as indicated in Figure 18. The sleeve plates not only facilitate the connection of the C-plates but also provide lateral bracing to the ends of the C-plates, thus reducing the possibility of lateral torsional buckling (LTB) of the C-plates. Also, the use of sleeve plates allows the forces from the C-plates to be transmitted to the centroid of the bracing members. This approach minimizes the risk of inducing LTB to the bracing members.



(a) interconnected holes to create the internal edge of the required "C" shape



(b) final smoothing of the internal edge of the C-plate

Figure 16. Fabrication procedure of a C-plate using a fixed drill to cut a commercially available steel strip.

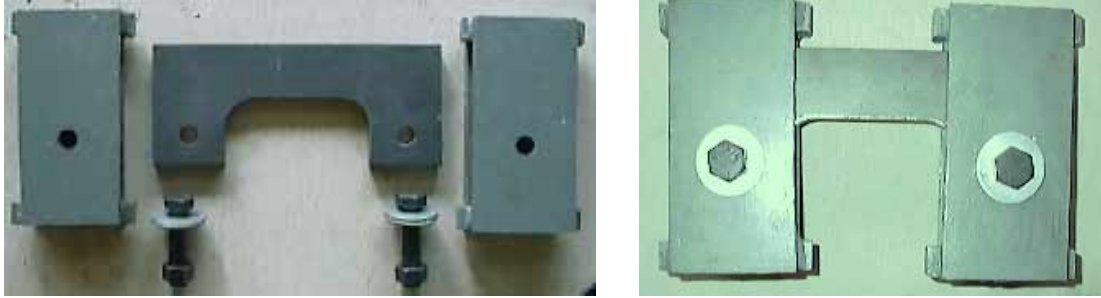
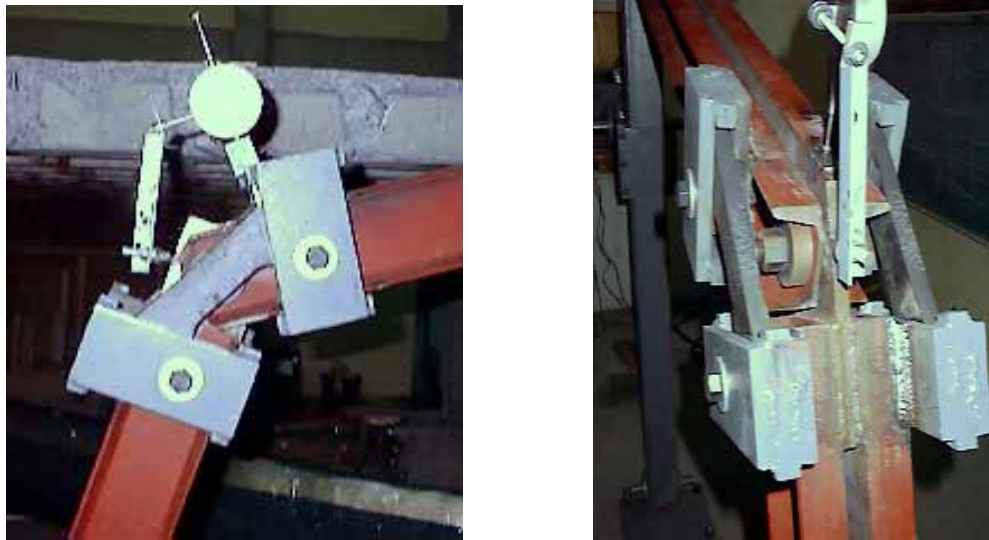


Figure 17. Assembly of sleeve plates and C-plates before the sleeve plates



(a) lateral view

(b) corner view

Figure 18. Yield devices at the end of the test

Results

The yield dissipative bracing was subjected to the same history of deformations applied to the frictional bracing. The same instrumentation was also used to measure jack pressure, rotations and displacements. The lack of a working data acquisition system inhibited the monitoring of strains both in the C-plates or the bracing members. Accordingly, the assessment of inelastic response is mostly based on observations of the global response of the bracing as described below.

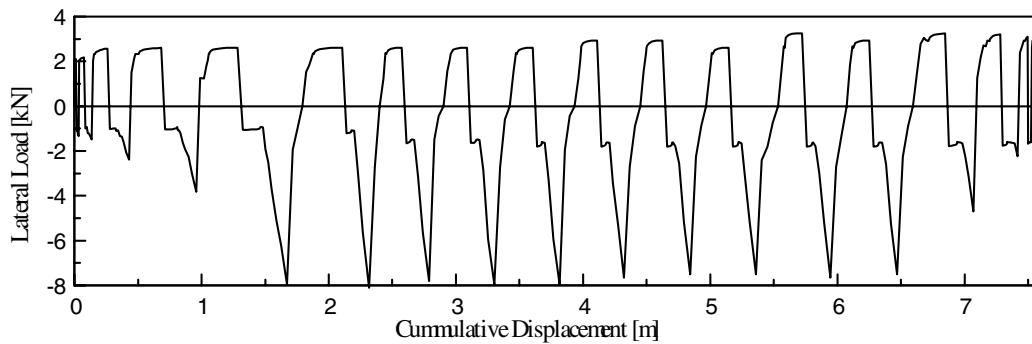


Figure 19. History of lateral strength of the yield dissipative bracing

Figure 19 shows the history of lateral strength of the frictional dissipative bracing under the applied history of displacements defined by Figure 11. In contrast with the behavior observed in the frictional bracing, the yield bracing presents asymmetrical response. However, despite this lack of symmetry the response is stable for the full range of displacements.

Figure 20a shows the hysteretic response observed in the yield dissipative bracing. Under compressive loading the response is bilinear with a mixture of cinematic and isotropic hardening. However, for storey drifts in excess of about 1%, the response under tensile loading appears to be strongly affected by both the material nonlinearities of the C-plate and the geometric nonlinearities favored by the central eccentricity e created along a fictitious diagonal joining the lower hinge with upper hinge of the bracing (Figure 14b). In other words, large displacements due to tension in the bracing system lead to a gradual increase of strength and stiffness. This occurs as a result of the significant reduction of the central eccentricity of the bracing and the increased participation of the axial response of the yielding region of the C-plate.

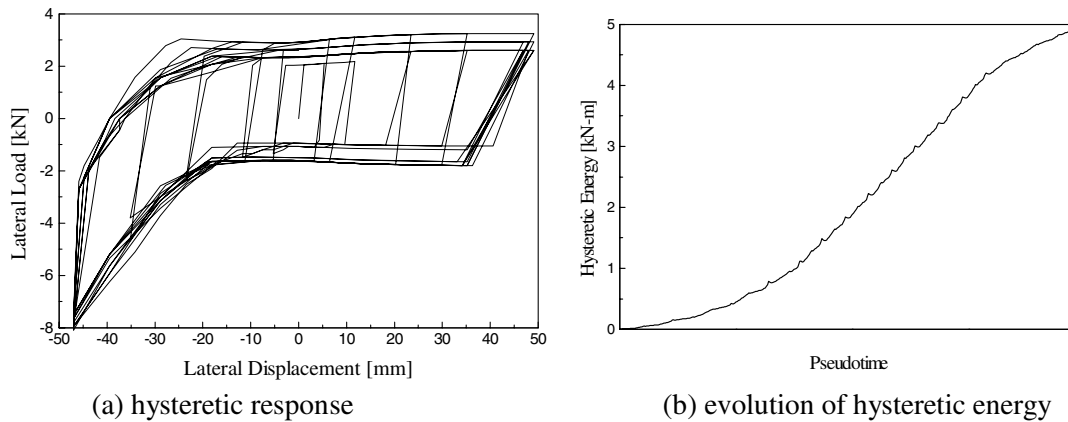


Figure 20. Hysteretic response of yield dissipative bracing

It is clear that a complete yield dissipative bracing (i.e. a complete polygonal arch) will exhibit symmetrical response as a result of having one half of the bracing working in tension and the other half working in compression. Nevertheless, the local increase of strength and stiffness that is achieved in the bracing region working in tension can be considered beneficial. In fact, this type of behavior at large displacements introduces an important amount of local recentering stiffness, improving the chances of the structure to return to its original position after a severe earthquake.



Figure 21. C-plate at the end of the test.

Although strains in the C-plates were not measured, the overall response of the yield dissipative bracing gives clear evidence of intense and stable inelastic response. At the end of the test the C-plates were subjected to a careful inspection (including the disassembly of the C-plates for better observation). As illustrated in Figures 18 and 21, yield bands were observed on the surface of the C-plates, primarily in the upper and bottom fibers of the dissipative region of the plates. No cracks visually observed at naked eye

were detected on the C-plates. Therefore, a careful 'low-tech' cutting procedure allows properly designed C-plates to achieve satisfactory inelastic response under cyclic loading of high amplitude. Also, no signs of yield or overstress were present in the surrounding regions of the holes for pinned connections in both the C-plates and the sleeve plates.

Figure 20b shows the evolution of the hysteretic energy dissipated by the C-plates. The plot shows a trend very similar to that observed in the frictional dissipative bracing. This confirms the observation [1,3] that the efficiency of a dissipative bracing of low invasivity is independent of the type of hysteretic devices used, as long as these devices are properly conceived, designed and constructed.

CONCLUDING REMARKS

The experimental program reported in this paper demonstrated that it is possible to design and construct an effective low invasivity dissipative bracing, making use of simple hysteretic devices of either friction or yield type, without resorting necessarily to high technology as commonly assumed.

The idea of a simultaneous activation of the yield and friction devices installed in the bracing tested in this research appears to be the most direct link to a yield-friction hybrid device. The development of this type of hysteretic device with dual energy dissipation characteristics merits further study.

ACKNOWLEDGEMENTS

The experimental program described in this paper was conducted by the author at his former institution, UAEM-Mexico with financial support from CONACYT. The author thanks Carlos Andrade Monteagudo for the fabrication of the test specimens and components of the loading system, Daniel Moreno for the fabrication of device components and Sergio Diaz Camacho for the materials testing. The author is also thankful to Cesar Villalta Iglesias, Juan Martinez Montes and Angelica Perel Garcia for their kind assistance during the several tests reported in this article.

REFERENCES

1. Martinez-Rueda J.E. "On the evolution of energy dissipation devices for seismic design." *Earthquake Spectra* 2002; 18(2): 309-346.
2. Martinez-Rueda J.E. "New eccentric bracing geometries for the passive control of earthquake-resistant structures." Proceedings of the 12th Mexican Conference on Seismic Engineering (in Spanish), SMIS, Mexico, 1999: 491-499.
3. Martinez-Rueda J.E. "Incorporation of hysteretic devices on bracing systems of low invasivity." CDROM Proceedings of the 13th World on Earthquake Engineering, Auckland, New Zealand, 2000.
4. Hoffman, G.W. Hoffmann, G.W., Kunnath, A.M., Reinhorn, A.M., and Mander, J.B. (1990) "Gravity-load-designed reinforced concrete buildings: seismic evaluation of existing construction and detailing strategies for improved seismic resistance," *Technical Report NCEER-92-0016*, National Center for Earthquake Engineering Research, State University of New York at Buffalo.
5. Martinez-Rueda J.E. "Analytic and experimental study of energy dissipation devices of low invasivity." CONACYT Research Report 31256U (in Spanish), Mexico, 2002.
6. Martinez-Rueda J.E. "Energy dissipation devices for seismic upgrading of RC structures." PhD Thesis, Civil Engineering Department, Imperial College of Science, Technology and Medicine, London, U.K., 1997
7. Mulas M.G. and Martinez-Rueda J.E. "Passive control in seismic retrofitting of steel MRFs." Proceedings of the 3rd World Conference on Structural Control, Como, Italy, 2002.
8. Ciampi, V., De Angelis, M. and Paolacci, F. "On the seismic design of dissipative bracing for seismic protection of structures." Proceedings of the 2nd European Conference on Structural Dynamics, Trondheim, Norway, 1993: 153-160.